Generalized coupled-mode formalism in reciprocal waveguides with gain, loss, anisotropy, or bianisotropy

Weijin Chen, Zhongfei Xiong, Jing Xu, and Yuntian Chen*
School of Optical and Electronic Information, Huazhong University of Science and Technology, Wuhan 430074, China

(Received 20 January 2018; revised manuscript received 29 April 2019; published 21 May 2019)

In anisotropic or bianisotropic waveguides, the standard coupled-mode theory fails due to the broken link between the forward- and backward-propagating modes, which together form the dual mode sets that are crucial in constructing coupled mode equations. We generalize the coupled-mode theory by treating the forward- and backward-propagating modes on the same footing via a generalized eigenvalue problem that is exactly equivalent to the waveguide Hamiltonian. The generalized eigenvalue problem is fully characterized by two operators, i.e., $(\bar{\boldsymbol{L}}, \bar{\boldsymbol{B}})$, wherein $\bar{\boldsymbol{L}}$ is a self-adjoint differential operator, while $\bar{\boldsymbol{B}}$ is a constant antisymmetric operator. From the properties of $\bar{\boldsymbol{L}}$ and $\bar{\boldsymbol{B}}$, we establish the relation between the dual mode sets that are essential in constructing coupled-mode equations in terms of forward- and backward-propagating modes. By perturbation, the generalized coupled-mode equation can be derived in a natural way. Our generalized coupled-mode formalism (GCMF) can be used to study the mode coupling in waveguides that may contain gain, loss, anisotropy, or bianisotropy. We further illustrate how the generalized coupled theory can be used to study the modal coupling in anisotropy and bianisotropy waveguides through a few concrete examples.

DOI: 10.1103/PhysRevB.99.195307

I. INTRODUCTION

Coupled mode theory (CMT) is an indispensable tool to analyze and design photonic devices, such as waveguides and cavities [1–12], and has far-reaching implications and applications in many subfields of optics [1–3,8,9,13–23]. CMT is a theoretical framework that treats each individual optical mode with certain spatiotemporal distributions as a single object, among which one mode could be coupled to another as the control parameter of the optical system, such as refractive indices or shapes of optical structures, varies. As a simple model, CMT provides not only an intuitive picture of how the photonic modes are hybridized, but also a quantitative assessment of how the hybridization among those relevant modes evolves. Especially, CMT in the waveguides has been a great tool to study the modal properties of various waveguides [1,2,24] as well as waveguide lattices [18,25]. In coupled waveguide-cavity systems [3,26,27], the temporal CMT [28] provides insight to design the ultrafast optical switch. Considering the recent development in metamaterials, man-made anisotropic mediums can be created, leading to interesting applications in controlling the flow and polarization of light [29]. Therefore, there is a large need to study waveguides that may contain anisotropy or bianisotropy.

In waveguide CMT, each mode characterized by the propagation constant β and the corresponding mode profile can be treated as a single object described as follows:

$$\mathcal{H}\boldsymbol{\phi} = \beta\boldsymbol{\phi}, \tag{1}$$

where $\mathcal{H}$ is the waveguide Hamiltonian. The construction of a coupled-mode equation of waveguides under certain perturbation $\mathcal{H}+\Delta$ takes three steps. First, the field of the perturbed waveguide is expanded as $\boldsymbol{\phi}^{\text{new}} = \sum a_i\boldsymbol{\phi}_i$, where all $\boldsymbol{\phi}_i$ functions span a complete mode set associated with Hamiltonian $\mathcal{H}$, i.e., the space of the right eigenstates $[\boldsymbol{\phi}_i]$; second, Eq. (1) of the perturbed system can be revised as a residual form $R = (\mathcal{H}+\Delta)\boldsymbol{\phi}^{\text{new}} - \beta\boldsymbol{\phi}^{\text{new}}$, which is further tested against all the possible $\boldsymbol{\psi}_j$ coined as the test functions that span the space of the left eigenstates $[\boldsymbol{\psi}_j]$ associated with Hamiltonian $\mathcal{H}$. Last, the link between the expansion functions $\boldsymbol{\phi}_i$ and the test functions $\boldsymbol{\psi}_j$ can be built within a proper inner product between $\boldsymbol{\phi}_i$ and $\boldsymbol{\psi}_j$, such that the coupled-mode equations can be constructed. The aforementioned procedure in constructing CMT has been used extensively in computational electromagnetism, such as the method of moments [30] and finite element method [31], which can be further proved to be exactly equivalent to the variational principle [31–37].

There are two different types of inner products, i.e., Hermitian inner products and bi-orthogonal products [38–40], both of which are heavily used in waveguide CMT. In the scheme of Hermitian inner products, it turns out that the left eigenstates $\boldsymbol{\psi}_j$ can be obtained by performing the Hermitian operation on the right eigenstates $\boldsymbol{\phi}_i$, implying the fact that the waveguide Hamiltonian $\mathcal{H}$ is a Hermitian operator and the integrated power flux flowing along propagation direction, i.e., z axis, of the waveguide is conserved [32,41,42]. In parallel, the left eigenstates $\boldsymbol{\psi}_j$ in a biorthogonal product can be obtained by performing the transpose operation and certain operations in field components of the right eigenstates $\boldsymbol{\phi}_i$, provided that the waveguide medium is reciprocal and the reaction conservation is fulfilled [42,43]. In the waveguide with gains and losses, the integrated power flux flowing along

*yuntian@hust.edu.cn

the waveguide is apparently not conserved, thus the modal coupling model based on the biorthogonal product is proposed by Xu *et al.* [43] to study $\mathcal{PT}$-symmetric waveguides that contain balanced gains and losses. Essentially, the general coupled-mode theory (GCMT) [43] is a revision of CMT by Haus [32], replacing the Hermitian inner product with the biorthogonal product, wherein the reciprocity or the reaction conservation still holds.

Physically, the expansion function $\boldsymbol{\phi}_i$ can be taken as the forward-propagating modes associated with the waveguide Hamiltonian $\mathcal{H}$, while the test function $\boldsymbol{\psi}_j$ corresponds to the time-reversal partner (backward-propagating modes) with respect to $\boldsymbol{\phi}_i$ in the scheme of Hermitian inner (biorthogonal) product. In either Hermitian inner product or biorthogonal product, the inner product between $\boldsymbol{\phi}_i$ and $\boldsymbol{\psi}_j$ yields a physical quantity that is independent of the z coordinate, such that the three-dimensional (3D) waveguide problem is reduced to a 2D counterpart. Such dimensional reduction is necessary, as it significantly reduces the computational load. In the biorthogonal product, such dimensional reduction in CMT works perfectly well for waveguides, in which the material is isotropic or only contains the in-plane anisotropy. In contrast, dimensional reduction is in conflict with the definite relation between the forward-propagating modes $\boldsymbol{\phi}_i$ with the backward-propagating modes $\boldsymbol{\psi}_j$, if the material tensor of a waveguide contains terms that couple the transverse components and longitudinal component. In a generic scenario, the definite relation between forward- and backward-propagating modes is lost. However, the coupled-mode equations in all the available CMT in literature are essentially constructed by testing Eq. (1) against all the possible $\boldsymbol{\psi}_j$, which is deduced from the expansion functions $\boldsymbol{\phi}_i$ [30–32,42,43] based on the aforementioned relation. Importantly, it is the completeness of the mode set $[\boldsymbol{\psi}_i]$ of test functions, i.e., all the possible $\boldsymbol{\psi}_j$, that guarantees the equivalence to the variational principle. In this regard, the completeness of $[\boldsymbol{\psi}_i]$ associated with the Hamiltonian $\mathcal{H}$ of the anisotropic/bianisotropic waveguides needs to be restored to construct the coupled-mode equations. In special cases, the forward- and backward-propagating modes are related by symmetry operations [44]. In a generic waveguide with bianisotropy, the relation between the forward- and backward-propagating modes is lost, which indicates that there is no definite relation between the expansion function $\boldsymbol{\phi}_j$ and the test function $\boldsymbol{\psi}_j$. Hence, the procedures in constructing the coupled-mode equations as given in literature [32] do not apply here. Notably, our discussion here is different from previous attempts on solving the modal coupling in homogeneous or partially filled bianisotropic metallic waveguide [45–48], where the expansion functions $\boldsymbol{\phi}_i$ are eigenmodes of the rectangular metallic waveguides filled with homogeneous isotropic achiral materials. The deficiency of this approach is the slow convergence with respect to the number of expansion functions, i.e., from a few tens at minimum to a few hundred, as well as the special boundary conditions (perfect electric conductor or perfect magnetic conductor) that are not applied for dielectric waveguides.

In this paper, we aim to develop a generalized CMT in photonic waveguide systems containing *gains, losses*, *anisotropy,* and *bianisotropy*, which can account for the modal coupling by including only *a few relevant modes* for both microwave waveguides and optical dielectric waveguides. We show that the standard CMT in those waveguides with anisotropy/bianisotropy fails due to the broken link between the forward- and backward-propagating modes. In our paper, we start with a formal description of the generalized eigenvalue problem of the bianisotropic waveguide by putting the forward- and backward-propagating modes on the same footing. Namely, the forward- and backward-propagating modes are combined together to constitute the complete expansion mode set $[\boldsymbol{\phi}_i]$. As for the reciprocal waveguide, it can be proved that the test function mode set $[\boldsymbol{\psi}_i]$ and expansion mode set $[\boldsymbol{\phi}_i]$ can be related. As a consequence, the coupled-mode equation can be constructed in a similar procedure as discussed previously. We show that our GCMF captures all the relevant features in the mode coupling in waveguides with anisotropy/bianisotropy through a few concrete examples.

This paper is organized as follows. In Sec. II, we reformulate the vectorial wave equation of the waveguide problem into a generalized eigenvalue problem $(\bar{\boldsymbol{L}}, \bar{\boldsymbol{B}})$. We further introduce the adjoint generalized eigenvalue problem $(\bar{\boldsymbol{L}}^a, \bar{\boldsymbol{B}}^a)$ under the biorthogonal product. In Sec. III, we examine the relation between the two complementary waveguide systems, i.e., $(\bar{\boldsymbol{L}}, \bar{\boldsymbol{B}})$ and $(\bar{\boldsymbol{L}}^a, \bar{\boldsymbol{B}}^a)$, in reciprocal waveguides. The symmetry relations between the modes associated with $(\bar{\boldsymbol{L}}, \bar{\boldsymbol{B}})$ and $(\bar{\boldsymbol{L}}^a, \bar{\boldsymbol{B}}^a)$ can be summarized by the *same-β argument* and the *pairing-β argument*. Based on the symmetry relations, we provide the procedures of constructing CMT, in which the forward- and backward-propagating modes are included in the modal expansion set. In Sec. IV, we apply our theory to study three examples, showing that our theory captures the features of the modal coupling due to the broken link between the forward- and backward-propagating modes. Section V concludes the paper.

II. GENERALIZED EIGENVALUE PROBLEM OF WAVEGUIDE

A. Generalized eigenvalue problem of original waveguide system

Throughout the paper, bold symbols with bars represent matrices or matrix operators, bold symbols correspond to vectors or vector operators, and normal symbols denote scalars. We consider a generic bianisotropic waveguide, in which the constitutive relation can be given as follows [49]:

$$\begin{aligned} \boldsymbol{D} &= \bar{\boldsymbol{\varepsilon}}\boldsymbol{E} + \bar{\boldsymbol{\chi}}_{eh}\boldsymbol{H}, \\ \boldsymbol{B} &= \bar{\boldsymbol{\mu}}\boldsymbol{H} + \bar{\boldsymbol{\chi}}_{he}\boldsymbol{E}, \end{aligned} \tag{2}$$

where $\boldsymbol{D}/\boldsymbol{B}$ is electric displacement/magnetic induction, $\boldsymbol{E}/\boldsymbol{H}$ is electric/magnetic field, respectively, $\bar{\boldsymbol{\varepsilon}} = \varepsilon_0\bar{\boldsymbol{\varepsilon}}_r$ $(\bar{\boldsymbol{\mu}} = \mu_0\bar{\boldsymbol{\mu}}_r)$ is permittivity (permeability) tensor, $\bar{\boldsymbol{\chi}}_{eh} = \sqrt{\varepsilon_0\mu_0}\bar{\boldsymbol{\chi}}_{r,eh}$ and $\bar{\boldsymbol{\chi}}_{he} = \sqrt{\varepsilon_0\mu_0}\bar{\boldsymbol{\chi}}_{r,he}$ are magnetoelectric coupling constants. Explicitly, $\bar{\boldsymbol{\varepsilon}}_r = \begin{pmatrix} \bar{\boldsymbol{\varepsilon}}_r^{tt} & \boldsymbol{\varepsilon}_r^{tz} \\ \boldsymbol{\varepsilon}_r^{zt} & \varepsilon_r^{zz} \end{pmatrix} = \begin{pmatrix} \varepsilon_r^{xx} & \varepsilon_r^{xy} & \varepsilon_r^{xz} \\ \varepsilon_r^{yx} & \varepsilon_r^{yy} & \varepsilon_r^{yz} \\ \varepsilon_r^{zx} & \varepsilon_r^{zy} & \varepsilon_r^{zz} \end{pmatrix}$, $\bar{\boldsymbol{\mu}}_r = \begin{pmatrix} \bar{\boldsymbol{\mu}}_r^{tt} & \boldsymbol{\mu}_r^{tz} \\ \boldsymbol{\mu}_r^{zt} & \mu_r^{zz} \end{pmatrix} = \begin{pmatrix} \mu_r^{xx} & \mu_r^{xy} & \mu_r^{xz} \\ \mu_r^{yx} & \mu_r^{yy} & \mu_r^{yz} \\ \mu_r^{zx} & \mu_r^{zy} & \mu_r^{zz} \end{pmatrix}$, $\bar{\boldsymbol{\chi}}_{r,he} = \begin{pmatrix} \bar{\boldsymbol{\chi}}_{r,he}^{tt} & \boldsymbol{\chi}_{r,he}^{tz} \\ \boldsymbol{\chi}_{r,he}^{zt} & \chi_{r,he}^{zz} \end{pmatrix} = i\begin{pmatrix} \chi_{r,he}^{xx} & \chi_{r,he}^{xy} & 0 \\ \chi_{r,he}^{yx} & \chi_{r,he}^{yy} & 0 \\ 0 & 0 & 0 \end{pmatrix}$, and $\bar{\boldsymbol{\chi}}_{r,eh} =$

$\begin{pmatrix} \bar{\chi}^{tt}_{r,eh} & \chi^{tz}_{r,eh} \\ \chi^{zt}_{r,eh} & \chi^{zz}_{r,eh} \end{pmatrix} = i\begin{pmatrix} \chi^{xx}_{r,eh} & \chi^{xy}_{r,eh} & 0 \\ \chi^{yx}_{r,eh} & \chi^{yy}_{r,eh} & 0 \\ 0 & 0 & 0 \end{pmatrix}$. Considering an infinitely long waveguide with translation symmetry along z, the waveguide modes can be obtained by solving the Maxwell's equation with a time harmonic dependence $e^{i\omega t}$, i.e., $\nabla \times \boldsymbol{E} = -i\omega(\bar{\boldsymbol{\mu}}\boldsymbol{H} + \bar{\boldsymbol{\chi}}_{he}\boldsymbol{E})$, $\nabla \times \boldsymbol{H} = i\omega(\bar{\boldsymbol{\varepsilon}}\boldsymbol{E} + \bar{\boldsymbol{\chi}}_{eh}\boldsymbol{H})$, where $i = \sqrt{-1}$. With normalization, i.e., $\boldsymbol{e} = \boldsymbol{E}$ and $\boldsymbol{h} = \sqrt{\frac{\mu_0}{\varepsilon_0}}\boldsymbol{H}$, we reformulate Maxwell's equations as follows:

$$\begin{aligned} \left[\nabla \times + ik_0\bar{\boldsymbol{\chi}}_{r,he}\right]\boldsymbol{e}_{3d}(x,y,z) + ik_0\bar{\boldsymbol{\mu}}_r\boldsymbol{h}_{3d}(x,y,z) = 0, \\ \left[\nabla \times - ik_0\bar{\boldsymbol{\chi}}_{r,eh}\right]\boldsymbol{h}_{3d}(x,y,z) - ik_0\bar{\boldsymbol{\varepsilon}}_r\boldsymbol{e}_{3d}(x,y,z) = 0, \end{aligned} \tag{3}$$

where vacuum wave number $k_0 = \omega\sqrt{\varepsilon_0\mu_0}$. By translation symmetry along z, the normalized electromagnetic field can be separated as the transverse terms and the longitudinal term, i.e., $\boldsymbol{e}_{3d}(x,y,z) = \boldsymbol{e}_{2d}(x,y)e^{-i\beta z} = \boldsymbol{e}^t_{2d}(x,y)e^{-i\beta z} + e^z_{2d}(x,y)e^{-i\beta z}$ ($\boldsymbol{h}_{3d}(x,y,z) = \boldsymbol{h}_{2d}(x,y)e^{-i\beta z} = \boldsymbol{h}^t_{2d}(x,y)e^{-i\beta z} + h^z_{2d}(x,y)e^{-i\beta z}$), where β is the propagation constant. Subsequently, Eqs. (3) can further be reformulated into a four-component equation by eliminating the longitudinal terms $e^z_{2d}(x,y)$ and $h^z_{2d}(x,y)$ via the expressions $e^z_{2d}(x,y) = \frac{\nabla_t \times \boldsymbol{h}^t_{2d}(x,y) - ik_0\boldsymbol{\epsilon}^{zt}_r \cdot \boldsymbol{e}^t_{2d}(x,y)}{ik_0\epsilon^{zz}_r}$ and $h^z_{2d}(x,y) = -\frac{\nabla_t \times \boldsymbol{e}^t_{2d}(x,y) + ik_0\boldsymbol{\mu}^{zt}_r \cdot \boldsymbol{h}^t_{2d}(x,y)}{ik_0\mu^{zz}_r}$, leading to the following equation given by

$$\bar{\boldsymbol{L}}\boldsymbol{\phi}_i = \beta_i\bar{\boldsymbol{B}}\boldsymbol{\phi}_i, \tag{4}$$

where

$$\bar{\boldsymbol{L}} = \begin{pmatrix} \boldsymbol{D}_1\frac{\boldsymbol{D}_2}{k_0\mu^{zz}_r} - k_0\bar{\boldsymbol{\varepsilon}}^{tt}_r + k_0\boldsymbol{\varepsilon}^{tz}_r\frac{\boldsymbol{\varepsilon}^{zt}_r}{\varepsilon^{zz}_r} & -k_0\bar{\boldsymbol{\chi}}^{tt}_{r,eh} + i\boldsymbol{D}_1\frac{\boldsymbol{\mu}^{zt}_r}{\mu^{zz}_r} + i\boldsymbol{\varepsilon}^{tz}_r\frac{\boldsymbol{D}_2}{\varepsilon^{zz}_r} \\ i\boldsymbol{D}_1\frac{\boldsymbol{\varepsilon}^{zt}_r}{\varepsilon^{zz}_r} + i\boldsymbol{\mu}^{tz}_r\frac{\boldsymbol{D}_2}{\mu^{zz}_r} + k_0\bar{\boldsymbol{\chi}}^{tt}_{r,he} & -\boldsymbol{D}_1\frac{\boldsymbol{D}_2}{k_0\varepsilon^{zz}_r} + k_0\bar{\boldsymbol{\mu}}^{tt}_r - k_0\boldsymbol{\mu}^{tz}_r\frac{\boldsymbol{\mu}^{zt}_r}{\mu^{zz}_r} \end{pmatrix}, \tag{5}$$

$\bar{\boldsymbol{B}} = \begin{bmatrix} 0 & 0 & 0 & -1 \\ 0 & 0 & 1 & 0 \\ 0 & -1 & 0 & 0 \\ 1 & 0 & 0 & 0 \end{bmatrix}$, $\boldsymbol{D}_1 = \begin{pmatrix} \frac{\partial}{\partial y} \\ -\frac{\partial}{\partial x} \end{pmatrix}$, $\boldsymbol{D}_2 = \begin{pmatrix} -\frac{\partial}{\partial y} & \frac{\partial}{\partial x} \end{pmatrix}$, $\boldsymbol{\phi} = [e_x, e_y, h_x, h_y]^T$, and T is the transpose operation. Equation (4) completely determines the series of waveguide modes labeled by i, with the propagation constant $\beta_i = n^i_{eff}k_0$, where n^i_{eff} is the ith effective modal index.

It is a trivial step to reformulate the generalized eigenvalue form in Eq. (4) to the Hamiltonian form given by Eq. (1), i.e., $\mathcal{H} = \bar{\boldsymbol{B}}^{-1}\bar{\boldsymbol{L}}$, as derived in our previous work [44]. The waveguide Hamiltonian $\mathcal{H}$ gives a concise and complete description of the waveguide [50], but involves complicated relations among the elements that are hard to interpret. In contrast, the generalized eigenvalue problem $(\bar{\boldsymbol{L}}, \bar{\boldsymbol{B}})$ shows a much more transparent relation among the elements in $(\bar{\boldsymbol{L}}, \bar{\boldsymbol{B}})$. It is easy to identify that $\bar{\boldsymbol{B}}$ is an antisymmetric matrix, i.e., $\bar{\boldsymbol{B}}^T = -\bar{\boldsymbol{B}}$, and some blocks in $\bar{\boldsymbol{L}}$ are symmetric matrices. Considering the complementary properties between $(\bar{\boldsymbol{L}}, \bar{\boldsymbol{B}})$ and $\mathcal{H}$, we will use both of them, where appropriate, to describe the waveguide system. The rationale behind will become clear in the following discussions of this paper.

B. Left eigenvector $\boldsymbol{\psi}^T_j$ and biorthogonal product

Equation (4) defines the right eigenvectors of $(\bar{\boldsymbol{L}}, \bar{\boldsymbol{B}})$, i.e., the expansion function $\boldsymbol{\phi}_i$ from the complete mode set $[\boldsymbol{\phi}_i]$. Similarly, the left eigenvector $\boldsymbol{\psi}$ is given by

$$\bar{\boldsymbol{L}}^T\boldsymbol{\psi}_j = \beta_j\bar{\boldsymbol{B}}^T\boldsymbol{\psi}_j, \tag{6}$$

where $\boldsymbol{\psi}_j$ has the same dimension as $\boldsymbol{\phi}_i$ but spans the complete mode set $[\boldsymbol{\psi}_j]$ associated with the test function space. Following Rumsey and Moiseyev [38,40], the biorthogonal inner product between $\boldsymbol{\phi}_i$ and $\boldsymbol{\psi}_j$ is defined as the following throughout the paper:

$$\langle\boldsymbol{\psi}_j, \boldsymbol{\phi}_i\rangle = \iint \boldsymbol{\psi}^T_j\boldsymbol{\phi}_i dV, \tag{7}$$

where $\boldsymbol{\phi}_i/\boldsymbol{\psi}_j$ is the expansion/test function. In the following part of this paper, the inner product defined in Eq. (7) is referred to as the first-type inner product throughout the paper. We further introduce the second-type inner product defined as follows:

$$\langle\boldsymbol{\psi}_j, \boldsymbol{\phi}_i\rangle_{\bar{\sigma}} = \iint \boldsymbol{\psi}^T_j\bar{\boldsymbol{\sigma}}\boldsymbol{\phi}_i dV, \tag{8}$$

where the metric tensor $\bar{\boldsymbol{\sigma}}$ equals $\bar{\boldsymbol{B}}$. The second-type inner product can be easily reduced to the first type if the metric tensor $\bar{\boldsymbol{\sigma}}$ is an identity matrix, thus the first inner is coined as the identity inner product, while the second inner product is coined as the B-inner product. It will be shown that the identity inner product is designed to work with the generalized eigenvalue description defined by $(\bar{\boldsymbol{L}}, \bar{\boldsymbol{B}})$, while the B-inner product works together with the Hamiltonian description of waveguide defined by $\mathcal{H}$.

C. Adjoint waveguide system

Provided the original waveguide described by $\mathcal{H}\boldsymbol{\phi}_i = \beta_i\boldsymbol{\phi}_i$, by definition the adjoint system $\mathcal{H}^a$ satisfies the following relation:

$$\langle\boldsymbol{\psi}_j, \mathcal{H}\boldsymbol{\phi}_i\rangle_{\bar{\boldsymbol{B}}} = \langle\mathcal{H}^a\boldsymbol{\psi}_j, \boldsymbol{\phi}_i\rangle_{\bar{\boldsymbol{B}}}, \tag{9}$$

for any $\boldsymbol{\phi}_i$ and $\boldsymbol{\psi}_j$ under the B-inner product. The equivalent generalized eigenvalue problem of adjoint system $\mathcal{H}^a$ can be given as follows:

$$\bar{\boldsymbol{L}}^a\boldsymbol{\psi}_j = \beta_j\bar{\boldsymbol{B}}^a\boldsymbol{\psi}_j, \tag{10}$$

where $\bar{\boldsymbol{B}}^a = \bar{\boldsymbol{B}}^T = -\bar{\boldsymbol{B}}$. Explicitly, right-hand side of Eq. (9) is equal to $\iint [(\bar{\boldsymbol{B}}^a)^{-1}\bar{\boldsymbol{L}}^a\boldsymbol{\psi}_j]^T\bar{\boldsymbol{B}}\boldsymbol{\phi}_i dV$, which can be reformulated as $\iint \boldsymbol{\psi}^T_j[\bar{\boldsymbol{L}}^a]^T[(\bar{\boldsymbol{B}}^a)^T]^{-1}\bar{\boldsymbol{B}}\boldsymbol{\phi}_i dV$. With the assistance of $[(\bar{\boldsymbol{B}}^a)^T]^{-1} = \bar{\boldsymbol{B}}^{-1}$, it is straightforward to prove that the adjoint relation given by Eq. (9) can be translated into the following relation:

$$\langle\boldsymbol{\psi}_j, \bar{\boldsymbol{L}}\boldsymbol{\phi}_i\rangle = \langle\bar{\boldsymbol{L}}^a\boldsymbol{\psi}_j, \boldsymbol{\phi}_i\rangle. \tag{11}$$

Equation (11) indicates that the adjoint relation between $(\bar{\boldsymbol{L}}, \bar{\boldsymbol{B}})$ and $(\bar{\boldsymbol{L}}^a, \bar{\boldsymbol{B}}^a)$ can be simplified into the adjoint relation between $\bar{\boldsymbol{L}}$ and $\bar{\boldsymbol{L}}^a$. At present, the adjoint operator $\bar{\boldsymbol{L}}^a$ is in an abstract form, and the concrete form of $\bar{\boldsymbol{L}}^a$ will be given in the next section.

III. RECIPROCAL WAVEGUIDES

In Sec. II, we have discussed that the adjoint waveguide system defined by $(\bar{\boldsymbol{L}}^a, -\bar{\boldsymbol{B}})$ can be related to the original waveguide system via Eq. (11), wherein $\bar{\boldsymbol{L}}^a$ is implicit. In this section, we continue to discuss the adjoint waveguide system of $(\bar{\boldsymbol{L}}, \bar{\boldsymbol{B}})$ and give explicit form of $\bar{\boldsymbol{L}}^a$ by reciprocity. We further study the orthogonal relation between the modes from the two complete mode sets $[\boldsymbol{\phi}_i]$ and $[\boldsymbol{\psi}_i]$.

$$\bar{\boldsymbol{L}}^a = \begin{pmatrix} \boldsymbol{D}_1 \frac{\boldsymbol{D}_2}{k_0 \mu_r^{a,zz}} - k_0 \bar{\boldsymbol{\varepsilon}}_r^{a,tt} + k_0 \boldsymbol{\varepsilon}_r^{a,tz} \frac{\boldsymbol{\varepsilon}_r^{a,zt}}{\varepsilon_r^{a,zz}} & -k_0 \bar{\boldsymbol{\chi}}_{r,eh}^{a,tt} + i\boldsymbol{D}_1 \frac{\boldsymbol{\mu}_r^{a,zt}}{\mu_r^{a,zz}} + i\boldsymbol{\varepsilon}_r^{a,tz} \frac{\boldsymbol{D}_2}{\varepsilon_r^{a,zz}} \\ i\boldsymbol{D}_1 \frac{\boldsymbol{\varepsilon}_r^{a,zt}}{\varepsilon_r^{a,zz}} + i\boldsymbol{\mu}_r^{a,tz} \frac{\boldsymbol{D}_2}{\mu_r^{a,zz}} + k_0 \bar{\boldsymbol{\chi}}_{r,he}^{a,tt} & -\boldsymbol{D}_1 \frac{\boldsymbol{D}_2}{k_0 \varepsilon_r^{a,zz}} + k_0 \bar{\boldsymbol{\mu}}_r^{a,tt} - k_0 \boldsymbol{\mu}_r^{a,tz} \frac{\boldsymbol{\mu}_r^{a,zt}}{\mu_r^{a,zz}} \end{pmatrix}, \tag{12}$$

where the material tensors $\bar{\boldsymbol{\varepsilon}}_r^a$, $\bar{\boldsymbol{\mu}}_r^a$, $\bar{\boldsymbol{\chi}}_{r,he}^{a,tt}$, $\bar{\boldsymbol{\chi}}_{r,eh}^{a,tt}$ are to be determined. According to the requirement imposed by the adjoint relation, i.e., Eq. (11), it is straightforward to identify the material tensors of the adjoint waveguides, i.e., $\bar{\boldsymbol{\varepsilon}}_r^a = \bar{\boldsymbol{\varepsilon}}_r^T$, $\bar{\boldsymbol{\mu}}_r^a = \bar{\boldsymbol{\mu}}_r^T$, $\bar{\boldsymbol{\chi}}_{r,he}^{a,tt} = -(\bar{\boldsymbol{\chi}}_{r,eh}^{tt})^T$, and $\bar{\boldsymbol{\chi}}_{r,eh}^{a,tt} = -(\bar{\boldsymbol{\chi}}_{r,he}^{tt})^T$. As for the reciprocal waveguide, the material tensors fulfill the reciprocity conditions, which require $\bar{\boldsymbol{\varepsilon}}_r = (\bar{\boldsymbol{\varepsilon}}_r)^T$, $\bar{\boldsymbol{\mu}}_r = (\bar{\boldsymbol{\mu}}_r)^T$, $\bar{\boldsymbol{\chi}}_{r,he} = -(\bar{\boldsymbol{\chi}}_{r,eh})^T$. As a result, it is trivial to find out that the following relation holds:

$$\langle \boldsymbol{\psi}_j, \bar{\boldsymbol{L}} \boldsymbol{\phi}_i \rangle = \langle \bar{\boldsymbol{L}} \boldsymbol{\psi}_j, \boldsymbol{\phi}_i \rangle, \tag{13}$$

which reveals that $\bar{\boldsymbol{L}}$ is self-adjoint under the biorthogonal product defined by Eq. (7). In contrast to the established equivalence of adjointness of the matrix form $\boldsymbol{H}$ of the Maxwell's equations in Xu's work [43] and Lorentz reciprocity, where $\boldsymbol{H}$ is 3D operator, the operator $\bar{\boldsymbol{L}}$ is a 2D differential operator. Interestingly, the self-adjointness of the operator $\bar{\boldsymbol{L}}$ is also a necessary and sufficient condition to material reciprocity. Thus, we refer Eq. (13) as the waveguide reciprocity.

The waveguide reciprocity for reciprocal waveguides is one of the important results of this paper, the relevance of which we shall discuss in relation with the generalized coupled-mode formalism in depth later. To this end, we first examine the orthogonal relations of the waveguide modes. Combining the original equation Eq. (4) and the adjoint equation Eq. (10) in the form of $\iint [\boldsymbol{\psi}_j \cdot (4) - (10) \cdot \boldsymbol{\phi}_i] dxdy$, it is straightforward to derive the following equation [51–53]:

$$\langle \boldsymbol{\psi}_j, \bar{\boldsymbol{L}} \boldsymbol{\phi}_i \rangle - \langle \bar{\boldsymbol{L}}^a \boldsymbol{\psi}_j, \boldsymbol{\phi}_i \rangle = (\beta_i - \beta_j) \langle \boldsymbol{\psi}_j, \bar{\boldsymbol{B}} \boldsymbol{\phi}_i \rangle. \tag{14}$$

Equation (14) is essentially corresponding to the Lorentz reciprocity, where the source terms are set to be zero. Since we are interested in the reciprocal waveguide, the waveguide reciprocity requires that the term on the left hand vanishes, leading to the orthogonal relation between $\boldsymbol{\phi}_i$ and $\boldsymbol{\psi}_j$ as follows:

$$(\beta_i - \beta_j) \iint \boldsymbol{\psi}_j^T \bar{\boldsymbol{B}} \boldsymbol{\phi}_i \, dxdy = 0. \tag{15}$$

For $\beta_i \neq \beta_j$, the term $\iint \boldsymbol{\psi}_j^T \bar{\boldsymbol{B}} \boldsymbol{\phi}_i \, dxdy$ has to vanish, i.e, $\iint \boldsymbol{\psi}_j^T \bar{\boldsymbol{B}} \boldsymbol{\phi}_i \, dxdy = 0$. With proper normalization, the formula Eq. (15) can be reformulated as follows:

$$\langle \boldsymbol{\psi}_j, \boldsymbol{\phi}_i \rangle_{\bar{\boldsymbol{B}}} = \delta_{ij}, \tag{16}$$

where δ_{ij} is Kronecker δ function. Equation (16) is referred to as the B-orthogonal relation [54] between the original field $\boldsymbol{\phi}_i$ and the adjoint field $\boldsymbol{\psi}_j$ in this paper. By writing out all the components of $\boldsymbol{\phi}_i$ and $\boldsymbol{\psi}_j$ explicitly, one finds out that $\iint \boldsymbol{\psi}_j^T \bar{\boldsymbol{B}} \boldsymbol{\phi}_i \, dxdy$ equals $\iint (\boldsymbol{e}_i^t \times \boldsymbol{h}_j^t - \boldsymbol{e}_j^t \times \boldsymbol{h}_i^t)_z \, dxdy$, which has the physical meaning of an unconjugated form of Poynting vector along the propagation direction [55].

A. Waveguide reciprocity and orthogonal relation

Considering the operator $\bar{\boldsymbol{L}}$ associated with the original waveguide problem described by Eq. (5), the adjoint operator $\bar{\boldsymbol{L}}^a$ can be readily given by the following form:

B. Symmetric modal relations between $\boldsymbol{\phi}_i$ and $\boldsymbol{\psi}_i$ in reciprocal waveguide

By definition of the adjoint operator, one can prove that the two complementary waveguide modes described by $(\bar{\boldsymbol{L}}^a, \bar{\boldsymbol{B}}^a)$ and $(\bar{\boldsymbol{L}}, \bar{\boldsymbol{B}})$ share the same eigenvalues β regardless of the self-adjointness of L, which is called the *same-β* argument onward in our paper, see proof in Appendix A. Explicitly, the *same-β* argument is described by

$$\bar{\boldsymbol{L}} \boldsymbol{\phi}_i = \beta_i \bar{\boldsymbol{B}} \boldsymbol{\phi}_i, \tag{17a}$$

$$\bar{\boldsymbol{L}}^a \boldsymbol{\psi}_i = \beta_i \bar{\boldsymbol{B}}^a \boldsymbol{\psi}_i, \tag{17b}$$

where the original field ϕ_i and the adjoint field ψ_i share the same β_i. As for reciprocal waveguide, i.e., $\bar{\boldsymbol{L}} = \bar{\boldsymbol{L}}^a$ and $\bar{\boldsymbol{B}}^a = -\bar{\boldsymbol{B}}$, Eq. (17b) can be reformulated as

$$\bar{\boldsymbol{L}} \boldsymbol{\psi}_i = -\beta_i \bar{\boldsymbol{B}} \boldsymbol{\psi}_i. \tag{18}$$

In comparison with Eq. (17a), Eq. (18) gives a different eigensolution $[-\beta_i, \boldsymbol{\psi}_i]$, apart from the eigensolution $[\beta_i, \boldsymbol{\phi}_i]$, both of which are directly associated with $(\bar{\boldsymbol{L}}, \bar{\boldsymbol{B}})$. The two different eigensolutions share the same absolute value of β_i but with different signs [56], which is called the *pairing-β* argument in this paper. Notably, the *pairing-β* argument also applies to the adjoint operator $(\bar{\boldsymbol{L}}^a, \bar{\boldsymbol{B}}^a)$ in reciprocal waveguides, meaning that if $[\beta_i, \boldsymbol{\psi}_i]$ is an eigensolution to $(\bar{\boldsymbol{L}}^a, \bar{\boldsymbol{B}}^a)$, see Eq. (17b), there must be a different solution $[-\beta_i, \boldsymbol{\phi}_i]$ which fulfills $\bar{\boldsymbol{L}}^a \boldsymbol{\phi}_i = -\beta_i \bar{\boldsymbol{B}}^a \boldsymbol{\phi}_i$.

Evident from the aforementioned discussions, there are two modes ($[\beta_i, \boldsymbol{\phi}_i]$ and $[-\beta_i, \boldsymbol{\psi}_i]$) related with the original waveguide defined by $(\bar{\boldsymbol{L}}, \bar{\boldsymbol{B}})$ for a given β_i. Importantly,

TABLE I. Symmetric relation of original field and adjoint field in the reciprocal waveguides with $\beta_i > 0$.

	Mode with β_i	Mode with $-\beta_i$
$(\bar{\boldsymbol{L}}, \bar{\boldsymbol{B}})$	$[\beta_i, \boldsymbol{\phi}_i]$	$[-\beta_i, \boldsymbol{\psi}_i]$
$(\bar{\boldsymbol{L}}^a, \bar{\boldsymbol{B}}^a)$	$[\beta_i, \boldsymbol{\psi}_i]$	$[-\beta_i, \boldsymbol{\phi}_i]$

the two modal fields ($[-\beta_i, \boldsymbol{\phi}_i]$ and $[\beta_i, \boldsymbol{\psi}_i]$) are also the solutions to $(\bar{\boldsymbol{L}}^a, \bar{\boldsymbol{B}}^a)$, but with the flipped sign of β_i. The inferred adjoint eigensolutions associated with $(\bar{\boldsymbol{L}}^a, \bar{\boldsymbol{B}}^a)$ from the known solutions of $(\bar{\boldsymbol{L}}, \bar{\boldsymbol{B}})$ can be a great help to construct coupled-mode equations in general bianisotropic waveguides. Under a small perturbation to the original waveguide, the perturbed eigensolution in the system can be expressed by the unperturbed eigensolutions. For example, in an original waveguide with $2+2$ solutions, $\boldsymbol{\phi}_1$, $\boldsymbol{\phi}_2$, $\boldsymbol{\psi}_3$, and $\boldsymbol{\psi}_4$, the approximate forward- and backward-propagating eigensolutions in the perturbed system are $\boldsymbol{\Phi} = (a_1\boldsymbol{\phi}_1 + a_2\boldsymbol{\phi}_2 + a_3\boldsymbol{\psi}_1 + a_4\boldsymbol{\psi}_2)$ and $\boldsymbol{\Psi} = (b_1\boldsymbol{\phi}_1 + b_2\boldsymbol{\phi}_2 + b_3\boldsymbol{\psi}_1 + b_4\boldsymbol{\psi}_2)$ with the propagating constants β and $-\beta$, respectively, where the unknown coefficients a_j and b_j have no definite relations. It is worth noting that the eigensolutions are vector fields in the transverse plane without the phase term $e^{-i\beta z}$, in contrast with the full 3D fields (see Sec. II A for more details).

The symmetric modal relations, dictated by the *same-β* argument and the *pairing-β* argument, are summarized compactly in Table I for reciprocal waveguides. The established symmetric relation in Table I is largely derived from the mathematical terms, which can also be interpreted with physical meanings. For a given β_i, i.e., $\beta_i > 0$ corresponding to the forward-propagating mode, the pairing modes given by $[\beta_i, \boldsymbol{\phi}_i]$ and $[-\beta_i, \boldsymbol{\psi}_i]$ are essentially the forward-backward-propagating waveguide modes. From *pairing-β* argument, one immediately realizes that the forward- and backward-propagating modes share the same absolute value of β. However, for a generic anisotropic/bianisotropic waveguide, there is no sign to show that the mode profiles of forward- and backward-propagating modes, i.e., $\boldsymbol{\phi}_i$ and $\boldsymbol{\psi}_i$, are necessarily the same or can be correlated.

In a few special cases, the forward- and backward-propagating modes can indeed be transformed into each other via additional symmetries [44], as tabulated in Table II, where the matrix form of the symmetry operation $\bar{\boldsymbol{\sigma}} = \begin{pmatrix} -1 & 0 & 0 & 0 \\ 0 & 1 & 0 & 0 \\ 0 & 0 & -1 & 0 \\ 0 & 0 & 0 & -1 \end{pmatrix}$ is introduced to describe the chiral transformation. In the table, the three types of symmetry operation, including chiral symmetry, time-reversal symmetry, and parity symmetry, and corresponding material constraints are listed, see detailed description in Appendix B. Once the symmetry relation between the forward- and backward-propagating modes is known, one is able to use the forward-propagating modes as the complete mode set to expand the field of the perturbed waveguide, and the backward-propagating modes as the test function to construct the coupled-mode equation rigorously. In Haus's CMT [32], the time-reversal operator $\mathcal{T}$ is used to infer $\boldsymbol{\psi}_i$ from $\boldsymbol{\phi}_i$, while the revised CMT in Xu's work [43] takes the advantage of the chiral symmetry to infer $\boldsymbol{\psi}_i$ from $\boldsymbol{\phi}_i$. The single mode set used in either Haus's CMT or Xu's work is the one spanned by $\boldsymbol{\phi}_i$, i.e., $[\boldsymbol{\phi}_i]$. In generically bianisotropic waveguides, the symmetric relation between the forward- and backward-propagating modes vanishes, thus there is no simple way to deduce the $\boldsymbol{\psi}_i$ from $\boldsymbol{\phi}_i$. In this scenario, one needs to combine $\boldsymbol{\psi}_i$ and $\boldsymbol{\phi}_i$ to form the complete mode set to construct CMT, which will be discussed in the next section.

C. Generalized coupled-mode formalism by perturbation

By perturbation, we construct the generalized coupled-mode equations that treat the forward-propagating modes and the backward-propagating modes on the same footing. Under a small perturbation on $\bar{\boldsymbol{L}}^{\#}$, i.e., $\bar{\boldsymbol{L}}^{\#} = \bar{\boldsymbol{L}} + \Delta\bar{\boldsymbol{L}}$, the eigenmodes $\boldsymbol{\Phi}$ associated with the perturbed waveguide $(\bar{\boldsymbol{L}}^{\#}, \bar{\boldsymbol{B}})$ can be expanded as the eigenmodes $\boldsymbol{\phi}_i$ of the unperturbed waveguide $(\bar{\boldsymbol{L}}, \bar{\boldsymbol{B}})$. Explicitly, the perturbed waveguide mode is given by $\boldsymbol{\Phi} = \sum a_i\boldsymbol{\phi}_i$, where a_i are the coefficients to be determined, and the corresponding eigenvalue changes from the original eigenvalue β_i into unknown β. By perturbation, the original system Eq. (4) can be written as perturbed eigenvalue equation $\bar{\boldsymbol{L}}^{\#}\boldsymbol{\Phi} = \beta\bar{\boldsymbol{B}}\boldsymbol{\Phi}$. It can be proven that the perturbed operator $\bar{\boldsymbol{L}}^{\#}$ and original operator $\bar{\boldsymbol{L}}$ also satisfy the waveguide reciprocity. According to the definition of $\bar{\boldsymbol{L}}^{\#}$, the formula $\langle\boldsymbol{\psi}_j, \bar{\boldsymbol{L}}\boldsymbol{\Phi}\rangle$ can be written as $\langle\boldsymbol{\psi}_j, [\bar{\boldsymbol{L}}^{\#} - \Delta\bar{\boldsymbol{L}}]\boldsymbol{\Phi}\rangle$. Substituting $\langle\boldsymbol{\psi}_j, [\bar{\boldsymbol{L}}^{\#} - \Delta\bar{\boldsymbol{L}}]\boldsymbol{\Phi}\rangle$ into Eq. (13) and dividing it into two parts, one can derive $\langle\boldsymbol{\psi}_j, \bar{\boldsymbol{L}}^{\#}\boldsymbol{\Phi}\rangle - \langle\bar{\boldsymbol{L}}\boldsymbol{\psi}_j, \boldsymbol{\Phi}\rangle = \langle\boldsymbol{\psi}_j, \Delta\bar{\boldsymbol{L}}\boldsymbol{\Phi}\rangle$. Omitting the small perturbed term $\langle\boldsymbol{\psi}_j, \Delta\bar{\boldsymbol{L}}\boldsymbol{\Phi}\rangle$ leads to the reciprocal relation,

$$\langle\boldsymbol{\psi}_j, \bar{\boldsymbol{L}}^{\#}\boldsymbol{\Phi}\rangle = \langle\bar{\boldsymbol{L}}\boldsymbol{\psi}_j, \boldsymbol{\Phi}\rangle, \tag{19}$$

where $\boldsymbol{\psi}_j$ is the adjoint modes associated with waveguide defined by $(\bar{\boldsymbol{L}}, -\bar{\boldsymbol{B}})$. Importantly, the complete mode set in $[\boldsymbol{\psi}_j]$ can be deduced from the known solutions of $\boldsymbol{\phi}_i$, as evident from the *same-β argument* and the *pairing-β argument* in our previous discussions.

Similar to the procedure of building Eq. (14), the generalized coupled-mode formulation can be obtained as

$$\langle\boldsymbol{\psi}_j, \bar{\boldsymbol{L}}^{\#}\boldsymbol{\Phi}\rangle - \langle\bar{\boldsymbol{L}}\boldsymbol{\psi}_j, \boldsymbol{\Phi}\rangle = (\beta - \beta_j)\langle\boldsymbol{\psi}_j, \bar{\boldsymbol{B}}\boldsymbol{\Phi}\rangle, \tag{20}$$

TABLE II. Symmetry relations of original field and adjoint field in the reciprocal waveguides.

Type	Operator	Symmetry relation	Constraints
Chiral symmetry	$\boldsymbol{\sigma}$	$\boldsymbol{\psi}_i(\boldsymbol{r}) = \bar{\boldsymbol{\sigma}}\boldsymbol{\phi}_i(\boldsymbol{r})$	$\boldsymbol{\varepsilon}_r^{zt} = \boldsymbol{\varepsilon}_r^{tz} = 0$, $\boldsymbol{\mu}_r^{zt} = \boldsymbol{\mu}_r^{tz} = 0$ and $\bar{\boldsymbol{\chi}} = 0$
Time-reverse symmetry	$\mathcal{T}$	$\boldsymbol{\psi}_i(\boldsymbol{r}) = \bar{\boldsymbol{\sigma}}(\boldsymbol{\phi}_i(\boldsymbol{r}))^*$	$\bar{\boldsymbol{\varepsilon}}_r$, $\bar{\boldsymbol{\mu}}_r$ and $\bar{\boldsymbol{\chi}}$ are real
Parity symmetry	$\mathcal{P}$	$\boldsymbol{\psi}_i(\boldsymbol{r}) = \bar{\boldsymbol{\sigma}}\boldsymbol{\phi}_i(-\boldsymbol{r})$	$\bar{\boldsymbol{\varepsilon}}_r(\boldsymbol{r}) = \bar{\boldsymbol{\varepsilon}}_r(-\boldsymbol{r})$, $\bar{\boldsymbol{\mu}}_r(\boldsymbol{r}) = \bar{\boldsymbol{\mu}}_r(-\boldsymbol{r})$ and $\bar{\boldsymbol{\chi}}(\boldsymbol{r}) = -\bar{\boldsymbol{\chi}}(-\boldsymbol{r})$

and by simplification its matrix form can be derived as follows:

$$\Sigma a_j[k_{ij} + b_{ij} - i(\beta_i - \beta)p_{ij}] = 0, \tag{21}$$

where the boundary term b_{ij} is given by $b_{ij} = -\frac{i}{\epsilon_r^{zz}} \oint [\boldsymbol{\varepsilon}_r^{zt} \boldsymbol{e}_i^t \boldsymbol{h}_j^t - (\boldsymbol{\epsilon}_r^{tz})^T \boldsymbol{e}_j^t \boldsymbol{h}_i^t] \cdot dl$, and the normalzied term p_{ij} is $p_{ij} = -i \iint \boldsymbol{z} \cdot (\boldsymbol{e}_j^t \times \boldsymbol{h}_i^t - \boldsymbol{e}_i^t \times \boldsymbol{h}_j^t)\, dxdy$. The coupling coefficient k_{ij} contains three terms, i.e., $k_{ij} = k_{ij}^1 + k_{ij}^2 + k_{ij}^3$. The first term k_{ij}^1 is conventional perturbation contributed from transverse electric field, $k_{ij}^1 = \iint -\frac{k_0}{\epsilon_r^{zz}} \boldsymbol{e}_j^t \cdot (\Delta\boldsymbol{\epsilon}_r^{tz}\boldsymbol{\epsilon}_r^{zt} + \boldsymbol{\epsilon}_r^{tz}\Delta\boldsymbol{\epsilon}_r^{zt} + \Delta\boldsymbol{\epsilon}_r^{tz}\Delta\boldsymbol{\epsilon}_r^{zt})\boldsymbol{e}_i^t dxdy$. The second term k_{ij}^2 stems from magnetoelectric coupling, i.e., $k_{ij}^2 = ik_0 \iint (\boldsymbol{e}_j^t \cdot \Delta\bar{\boldsymbol{\chi}}_{r,eh}^{tt} \boldsymbol{h}_i^t + \boldsymbol{e}_i^t \cdot \Delta\bar{\boldsymbol{\chi}}_{r,eh}^{tt} \boldsymbol{h}_j^t)\, dxdy$, which could be particularly useful to study the mode hybridization in bianisotropic waveguides. The last term k_{ij}^3 is contributed from the coupling between the transverse field components and longitudinal field components, i.e., $k_{ij}^3 = \iint \frac{k_0}{\varepsilon_r^{zz}} [\boldsymbol{e}_i^t \cdot \Delta\boldsymbol{\varepsilon}_r^{tz}(\boldsymbol{\varepsilon}_r^{zt}\boldsymbol{e}_j^t + \varepsilon_r^{zz}e_j^z) + \boldsymbol{e}_j^t \cdot \Delta\boldsymbol{\varepsilon}_r^{tz}(\boldsymbol{\varepsilon}_r^{zt}\boldsymbol{e}_i^t + \varepsilon_r^{zz}e_i^z)]\, dxdy$.

Close examination shows that b_{ij} in Eq. (21) vanishes, thus the generalized coupled-mode equation of Eq. (21) can be reduced as

$$\sum_j a_j(\beta_j p_{ij} - ik_{ij}) = \beta \sum_j a_j p_{ij}, \tag{22}$$

where β is the propagation constant and a_j is the modal expansion coefficient. The present coupled-mode equation resembles the same matrix form as in Haus's CMT, as well as that in our own paper. However, it is worth emphasizing that both the forward- and backward-propagating modes are included in the mode expansion set in our formula Eq. (22). We will refer to Eq. (22) as GCMF to be distinct from previous coupled-mode equations, typically from Haus and ours [32,43].

As an example, we give the explicit matrix form of GCMF for two-mode hybridization, in which the definite relation between the forward- and backward-propagating modes does not exist under the perturbation. In this regard, there are four modes, i.e., two forward-propagating modes $(\boldsymbol{\phi}_1, \boldsymbol{\phi}_2)$ and two backward-propagating modes $(\boldsymbol{\psi}_1, \boldsymbol{\psi}_2)$, spanning the complete expansion mode set. Meanwhile, reciprocity guarantees that the mode set associated with the adjoint waveguide system $(\bar{\boldsymbol{L}}^a, \bar{\boldsymbol{B}}^a)$ is the same as that of $(\bar{\boldsymbol{L}}, \bar{\boldsymbol{B}})$ due to the fact that $\bar{\boldsymbol{L}}^a = \bar{\boldsymbol{L}}$, and $\bar{\boldsymbol{B}}^a = -\bar{\boldsymbol{B}}$. Therefore, the test function can be simply chosen from the four modes $\boldsymbol{\phi}_1$, $\boldsymbol{\phi}_2$, $\boldsymbol{\psi}_1$, $\boldsymbol{\psi}_2$. The eigenmode of the perturbed waveguide is given by $\boldsymbol{\Phi} = a_1\boldsymbol{\phi}_1 + a_2\boldsymbol{\phi}_2 + a_3\boldsymbol{\psi}_1 + a_4\boldsymbol{\psi}_2$, in which the coefficients a_j and the propagation constant β can be determined by the following coupled mode equation:

$$\begin{pmatrix} \beta_1 p_{11} - ik_{11} & \beta_2 p_{12} - ik_{12} & \beta_3 p_{13} - ik_{13} & \beta_4 p_{14} - ik_{14} \\ \beta_1 p_{21} - ik_{21} & \beta_2 p_{22} - ik_{22} & \beta_3 p_{23} - ik_{23} & \beta_4 p_{24} - ik_{24} \\ \beta_1 p_{31} - ik_{31} & \beta_2 p_{32} - ik_{32} & \beta_3 p_{33} - ik_{33} & \beta_4 p_{34} - ik_{34} \\ \beta_1 p_{41} - ik_{41} & \beta_2 p_{42} - ik_{42} & \beta_3 p_{43} - ik_{43} & \beta_4 p_{44} - ik_{44} \end{pmatrix} \begin{pmatrix} a_1 \\ a_2 \\ a_3 \\ a_4 \end{pmatrix} = \beta \begin{pmatrix} p_{11} & p_{12} & p_{13} & p_{14} \\ p_{21} & p_{22} & p_{23} & p_{24} \\ p_{31} & p_{32} & p_{33} & p_{34} \\ p_{41} & p_{42} & p_{43} & p_{44} \end{pmatrix} \begin{pmatrix} a_1 \\ a_2 \\ a_3 \\ a_4 \end{pmatrix}. \tag{23}$$

IV. RESULTS AND DISCUSSIONS

In this section, we apply the generalized coupled mode equation, i.e., Eq. (22), to study the modal coupling in anisotropic and bianisotropic waveguide that may contain gains and losses.

A. Anisotropic waveguide

In the first example, we study the anisotropic waveguide, the cross section of which is an anisotropic dielectric ellipse surrounded by a perfect electric conductor with long axis $a = \lambda_0$ and short axis $b = 0.5\lambda_0$ [see waveguide structure in Fig. 1(a)]. The dielectric tensor of waveguide core is anisotropic, i.e., $\bar{\boldsymbol{\varepsilon}}_r = \begin{pmatrix} 1 & 0 & \varepsilon_r \\ 0 & 1 & 0 \\ \varepsilon_r & 0 & 0.8 \end{pmatrix}$. Without loss of generality, the ε_r^{zz} is equal to 0.8 to ensure the single-mode operation, where only the coupling between the forward- and backward-propagating modes can exist. In Fig. 1(b), the dispersion of waveguide, i.e., the real and imaginary part of the effective refractive index (marked by red and black lines, respectively), is calculated by full-wave finite element modeling using commercial software package COMSOL MULTIPHYSICS [57]. In the range $\varepsilon_r = -0.7 \sim -0.45$ and $0.45 \sim 0.7$, the waveguide has real eigenvalues, i.e., $\mathrm{Im}(n_{\mathrm{eff}}) = 0$, shown by the red line, while in the range $\varepsilon_r = -0.45 \sim 0.45$ the effective modal indices become complex, i.e., $\mathrm{Im}(n_{\mathrm{eff}}) \neq 0$. The varied parameter ε_r at two junction points that separate the three ranges in Fig. 1(b) are identical, which are known as exceptional points (EPs). The phenomenon in waveguide systems has been extensively studied in the last few years. In a large scenario, the related research is coined $\mathcal{PT}$-symmetric photonics. In contrast to previous waveguide systems, which usually contain balanced gains and losses, the $\mathcal{PT}$-symmetry breaking in our waveguide is counterintuitive due to the fact that the waveguide here only contains anisotropy rather than balanced gains and losses. The same sign of ε_r^{xz} and ε_r^{zx} may be the reason for the imaginary eigenvalue, the underlying physics behind this phenomenon is beyond the scope of this paper. In the following, we will apply our GCMF from perturbation to examine the modal coupling in this waveguide. In particular, we select a limited region between two purple dashed lines, i.e., the range $\varepsilon_r = -0.5 \sim -0.4$, which contains an EP point, to compare n_{eff} predicted by our approach GCMF against the full-wave simulation. The selection of the region is not essential, GCMF can be applied in other regions as long as the perturbation is valid.

For simplicity, the dielectric tensor is rewritten as $\bar{\boldsymbol{\varepsilon}}_r = \begin{pmatrix} 1 & 0 & -0.5 \\ 0 & 1 & 0 \\ -0.5 & 0 & 0.8 \end{pmatrix} + \Delta\varepsilon \begin{pmatrix} 0 & 0 & 1 \\ 0 & 0 & 0 \\ 1 & 0 & 0 \end{pmatrix}$, where $\Delta\varepsilon$ is the strength of the perturbation accounting for the magnitude of anisotropy in the off-diagonal terms in $\bar{\boldsymbol{\varepsilon}}_r$. The modal indices between forward- and backward-propagating modes are symmetric with respect to $n_{\mathrm{eff}} = 0$ due to the *pairing-β argument* in reciprocal waveguides, which also holds in this example.

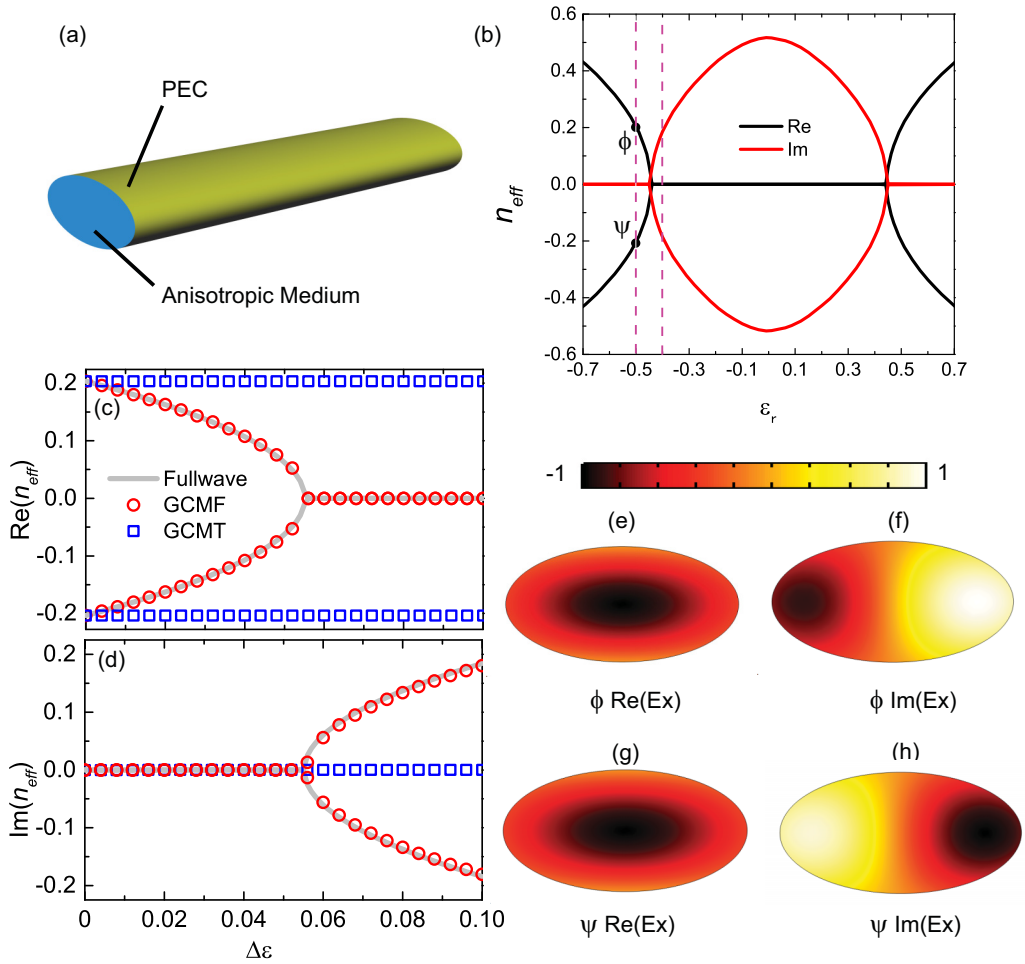

FIG. 1. (a) The schematic of elliptical waveguide with perfect electric conductor boundary with long axis $a = \lambda_0$ and short axis $b = 0.5\lambda_0$, where λ_0 is vacuum wavelength. (b) The real (red line) and imaginary (black line) part of effective modal indices, calculated from full-wave simulation using finite element method, as a function of ε_r. The two purple dashed lines in (b) indicate the range of ε_r, where GCMT and GCMF are applied. In (c) and (d), the real and imaginary parts of effective modal indices n_{eff} as a function of increased magnitude of anisotropy $\Delta\varepsilon$ for forward/backward-propagating modes, calculated from GCMF (red open circles), GCMT [43], (blue open squares), and full-wave simulation (gray line) are shown. In (e) and (f) [and (g) and (h)], the real/imaginary parts of Ex obtained from full-wave simulation is shown for the modes ϕ [and ψ], respectively, at $\varepsilon_r = -0.5$ marked by solid circle in (b).

As can be seen from Figs. 1(c)–1(d), the dispersion obtained from GCMF (red circles) shows excellent agreement with the numerical results from the full-wave simulations, but with a large discrepancy with that obtained from GCMT [43] (blue squares).

The discrepancy stems from the broken link between the forward- and backward-propagating modes, i.e., the chiral symmetry, which has been used implicitly to construct coupled-mode equations in Xu's work. To display the broken chiral symmetry, forward- and backward-propagation modes calculated by full-wave simulation is shown in Figs. 1(e)–1(h), where Figs. 1(e) and 1(f) plot the real/imaginary E_x part of forward-propagating mode ϕ, and Figs. 1(g) and 1(h) plot corresponding component of backward-propagating mode ψ, which are marked by black solid circles at $\varepsilon_r = -0.5$ in Fig. 1(b). The opposite imaginary parts of E_x in Figs. 1(f) and 1(h) clearly show the broken chiral symmetry. The same conclusion can also be drawn from the simple analysis on the relation between the field components and the propagation constant as follows. Due to the presence of the off-diagonal terms in the dielectric tensor, the transverse components $\boldsymbol{e}_t$ of the electric field of the waveguide mode are coupled to the longitudinal component e_z. Notably, the intrinsic spin-momentum locking of waveguide modes [58] gives rise to β-dependent relation between transverse components $\boldsymbol{e}_t$ and longitudinal component e_z. The relation between transversal and longitudinal electromagnetic components can be written as $e^z = \frac{(\nabla_t \cdot \bar{\boldsymbol{\varepsilon}}_r^{tt})\boldsymbol{e}^t + \nabla_t \cdot \boldsymbol{\varepsilon}_r^{tz} e^z}{i\beta\varepsilon_r^{zz}} - \frac{\boldsymbol{\varepsilon}_r^{zt}\boldsymbol{e}^t}{\varepsilon_r^{zz}}$, $h^z = \frac{\nabla_t \cdot \boldsymbol{h}^t}{i\beta}$. Supposing that the in-plane electric fields $\boldsymbol{e}^t$ of forward- and backward-propagation modes are identical, the longitudinal component is reduced to $e^z = \frac{(\nabla_t \cdot \bar{\boldsymbol{\varepsilon}}_r^{tt})\boldsymbol{e}^t}{i\beta\varepsilon_r^{zz}}$ when the constraints of chiral symmetry, i.e., $\boldsymbol{\varepsilon}_r^{zt} = 0$ and $\boldsymbol{\varepsilon}_r^{tz} = 0$, are satisfied. However, e^z of the forward- and backward-propagating modes are not opposite, if $\boldsymbol{\varepsilon}_r^{zt}$ and $\boldsymbol{\varepsilon}_r^{tz}$ exist. Evidently, the simple analysis as well as the comparison in Fig. 1(e)-1(h) shows that the definite relation

between forward- and backward-propagating modes is indeed lost, which can potentially compromise the validity of the CMT where only single-mode set is concerned.

B. Bianisotropic waveguide

In the second example, we consider a bianisotropic metamaterial waveguide, which can be realized by aligning electrically small split-ring resonators along a particular direction, see details in Xu's paper [49]. In this reciprocal waveguide, the geometric configuration is identical to a conventional waveguide with high material index in the core surrounded by air. In addition, the core layer contains bianisotropy, which is described by Eq. (2) with $\varepsilon_r = 4$, $\mu_r = 1$, and $\bar{\boldsymbol{\chi}}_{r,eh} = -\left(\bar{\boldsymbol{\chi}}_{r,he}\right)^T = \begin{pmatrix} 0 & i\Delta\chi & 0 \\ 0 & 0 & 0 \\ 0 & 0 & 0 \end{pmatrix}$, where $\Delta\chi$ is a positive number. The purpose of studying this typical bianisotropic waveguide is to illustrate the relevance of including the backward-propagating modes in the modal expansion set to obtain the correct modal hybridization, which will become clear shortly.

In this bianisotropic waveguide, there are two forward-propagating modes, i.e., the x-polarized mode and y-polarized mode. Due to the presence of $\Delta\chi$, the two components D_x and B_y have changed from original electric displacement $\boldsymbol{D}$ and magnetic field $\boldsymbol{B}$, i.e., $D_x = \varepsilon_0(\varepsilon_{11}e_x + i\chi_{12}h_y)$ and $B_y = \mu_0(-i\chi_{12}e_x + \mu_{22}h_y)$. So the x-polarized mode dominated by E_x and H_y are strongly modified due to χ_{12}. In contrast, the y-polarized mode dominated by E_y and H_x will not be affected at all, which is not shown here. We apply GCMF to study the mode hybridization in Fig. 2(a), which shows the effective modal index as function of $\Delta\chi$. The red symbols representing modal indices calculated by GCMF match well with the gray line obtained by full-wave simulations. Apparently, the *pairing-β argument* still applies. And the absolute value of modal index $|n_{\text{eff}}|$ decreases for larger $\Delta\chi$, see detailed explanation in Xu's work [49].

Though the x-polarized mode and y-polarized mode are completely decoupled as $\Delta\chi$ varies, the forward-propagating x-polarized mode and the backward-propagating mode are coupled together. In the implementation of GCMF, the y-polarized mode has been excluded, thus the complete modal set in constructing GCMF contains two modes, which are the forward- and backward-propagating x-polarized modes, i.e., $\boldsymbol{\phi}_1$, $\boldsymbol{\psi}_2$. Under perturbation, the two hybridized modes can be given by $\boldsymbol{\Phi}_1 = a_{11}\boldsymbol{\phi}_1 + a_{12}\boldsymbol{\psi}_2$, $\boldsymbol{\Psi}_2 = a_{21}\boldsymbol{\phi}_1 + a_{22}\boldsymbol{\psi}_2$, where the cross modal coefficient a_{12} (a_{21}) refers to the contribution from backward- (forward-) propagating mode $\boldsymbol{\psi}_2$ ($\boldsymbol{\phi}_1$) to the newly hybridized forward (backward) propagating mode $\boldsymbol{\Phi}_1$ ($\boldsymbol{\Psi}_2$). Figure 2(b) shows the normalized modal coefficients obtained from GCMF in the modal hybridization between the forward- and backward-propagating x-polarized mode. The modal coefficients a_{ij} are complex numbers, here only the absolute values of a_{ij} are shown. Apparently, the diagonal terms a_{11} and a_{22} are dominating, while the off-diagonal terms a_{12} and a_{21}, up to 4%, are not negligible, see Fig. 2(b). The non-negligible value of a_{12} indeed confirms our expectation that the backward-propagating mode will contribute to the forward-propagating mode in the modal hybridization under perturbation of $\Delta\chi$, and vice versa.

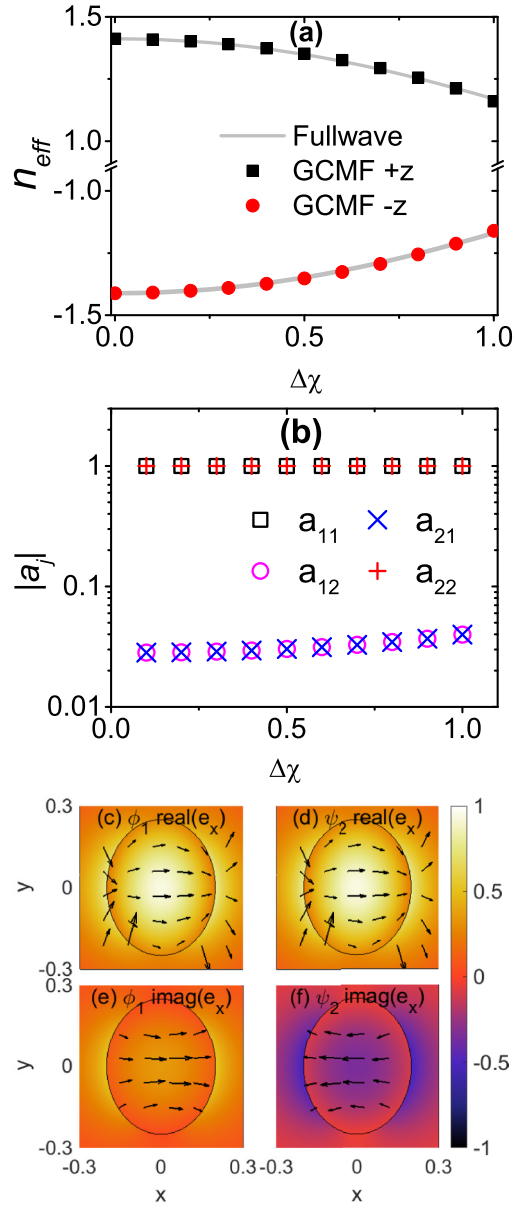

FIG. 2. Effective modal indices n_{eff} as function of the magneto-electric coupling ($\Delta\chi$) that accounts for the bianisotropy. The cross section of the waveguide is elliptical, with long (short) axis $a = 0.25\lambda_0$ ($b = 0.2\lambda_0$). In (a), the n_{eff} of forward/backward-propagating x-polarized mode is denoted by black/red solid circles. The gray solid lines are calculated from full-wave simulations. (b) shows modal coefficients of the hybridized mode upon a small perturbation, as $\Delta\chi$ varies. The real part of x component of forward/backward normalized electric field is shown in (c) and (d), and the vector plots of the real part of in-plane electric field are also shown in (c) and (d) indicated by the arrows, the length of which is proportional to the magnitude of the vector field. (e), (f) show the imaginary part of field, and the other setting is same to (c) and (d). In (c)–(f), the field profiles are obtained from COMSOL at $\Delta\chi = 0.4$.

Figures 2(c)–2(f) show the broken chiral symmetry, illustrating that GCMT could not apply to this example. In Figs. 2(c) and 2(e), the real/imaginary part of e_x component and the transversal field vector $\boldsymbol{e}^t$ for forward-propagating

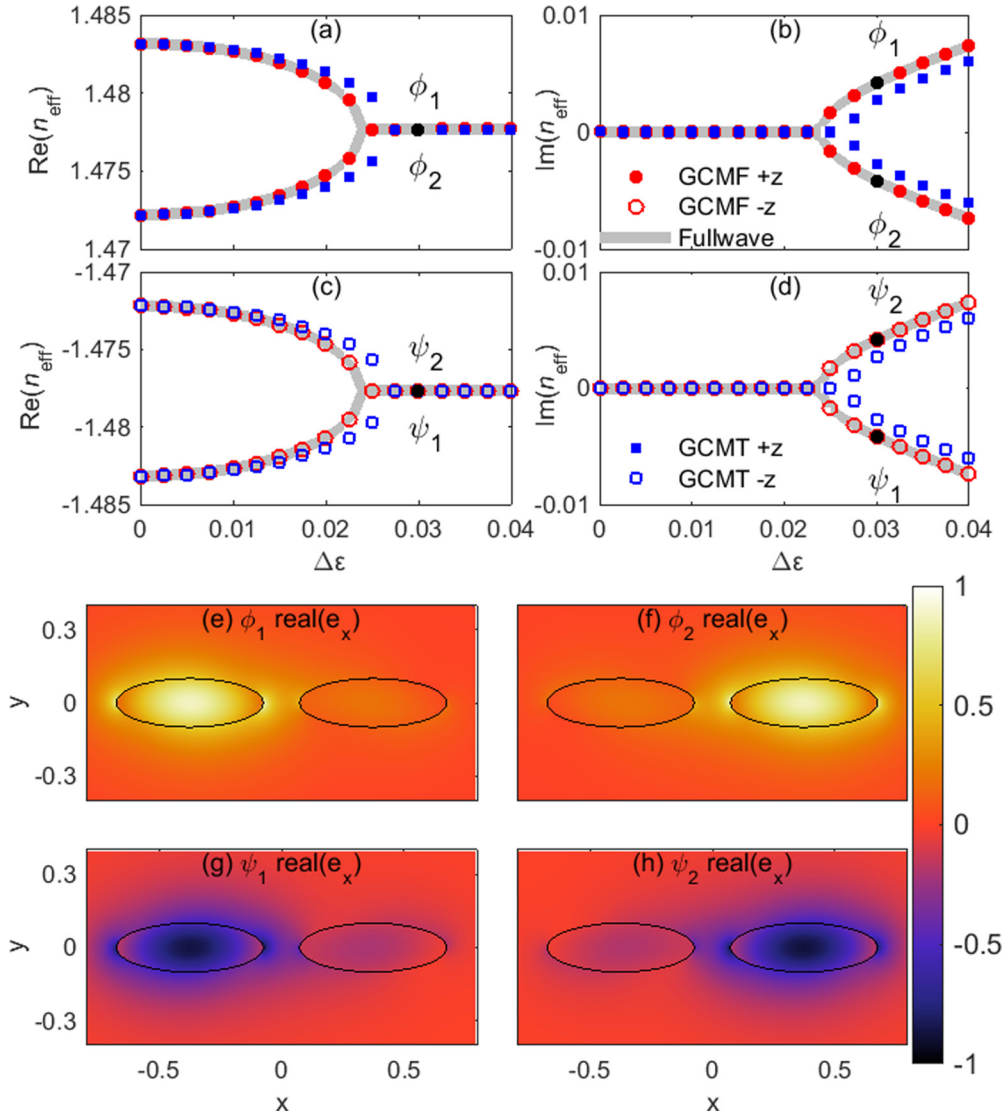

FIG. 3. Effective mode indices n_{eff} versus perturbation $\Delta\varepsilon$ using GCMF, GCMT, and full-wave simulation. The structure is a double elliptical waveguide with long axis $a = 0.3\lambda_0$, short axis $b = 0.1\lambda_0$, and the center distance $d = 0.75\lambda_0$. The red/blue/gray markers represent the results from GCMF/GCMT/full wave simulations, respectively. The (a), (b) and (c), (d) represent forward/backward-propagating modes n_{eff}, respectively. (a), (c) and (b), (d) represent real/imaginary parts of n_{eff}, respectively. The normalized Re(e_x) at $\Delta\varepsilon = 0.03$ calculated by GCMF are shown in (e)–(h), where (e), (f) for Re(e_x) of forward-propagating mode 1/2, and (g),(h) for Re(e_x) of backward-propagating mode 1/2.

field, which are obtained from COMSOL, are plotted. And in Figs. 2(d) and 2(f), the corresponding field of backward-propagating mode is shown. Similarly, the real parts and the opposite imaginary parts of e_x evidently show the broken chiral symmetry. As investigated in our previous work [44], the forward- and backward-propagating modes are time-reversal pairs, which can also be seen from Figs. 2(c)–2(f). Once the coupled-mode equation is implemented in the Hermitian inner product, the expansion modal set shall contain only one mode, which is enough due to the time-reversal symmetry. In the next section, we will continue to study waveguides containing gains, losses, as well as bianisotropy, in which both the chiral symmetry and the time reversal symmetry are broken. In those generically bianisotropic waveguides, the formal construction of the coupled-mode equations is to simultaneously include the forward- and backward-propagating modes in the modal expansion set.

C. Bianisotropic waveguide with $\mathcal{PT}$-symmetric gains and losses

The third example is a $\mathcal{PT}$-symmetry optical system with balanced gains and losses, as well as bianisotropy. The structure contains two identical single-mode elliptical waveguides surrounded by the air cladding, see Fig. 3. The material in the left elliptical guide is $\varepsilon_r = 4 + i\Delta\varepsilon$, $\chi^{xx}_{r,eh} = -\chi^{xx}_{r,he} = 1$, and in the right elliptical guide is $\varepsilon_r = 4 - i\Delta\varepsilon$, $\chi^{xx}_{r,eh} = -\chi^{xx}_{r,he} = -1$. The magnetoelectric coupling terms χ in the two elliptical waveguides are opposite to make this system to exhibit $\mathcal{PT}$

symmetry, i.e., $\mathcal{PT}\bar{\boldsymbol{L}}(\mathcal{PT})^{-1} = \bar{\boldsymbol{L}}$ (see detail in Xiong's work [44]).

The unperturbed system has two supermodes, an odd mode and an even mode, which are hybridized by two identical modes from two single-mode waveguides. These two modes are coupled by the gain/loss perturbation $i\Delta\varepsilon$, which is a parameter to measure the non-Hermiticity of this system [59]. As the parameter $\Delta\varepsilon$ increases, the system undergoes a transition from a completely real spectrum into a complex spectrum, which is known as $\mathcal{PT}$-symmetry breaking [60,61]. In Figs. 3(a) and 3(b), the n_{eff}s of two modes obtained from GCMF are real numbers representing exact $\mathcal{PT}$ symmetry before the EP $\Delta\varepsilon = 0.024$, while n_{eff}s of two modes become the complex conjugate pair after the exceptional point. In Figs. 3(c) and 3(d), the backward-propagating modes show exactly the same phenomenon.

As the $\mathcal{PT}$-symmetry breaking occurs, two conjugated modes (two forward-propagating modes or two backward-propagating modes) can be obtained from one another under the subsequent $\mathcal{P}$ ($\boldsymbol{r} \to -\boldsymbol{r}$) and $\mathcal{T}$ (complex conjugate) operations. In Figs 3(c)–3(f), $\boldsymbol{\phi}_1$ and $\boldsymbol{\phi}_2$ are two forward-propagating modes which satisfy relation $\boldsymbol{\phi}_1(r) = \boldsymbol{\phi}_2^*(-r)$. And in Figs. 3(g)–3(h), the backward-propagating modes $\boldsymbol{\psi}_1$ and $\boldsymbol{\psi}_2$ satisfy the same symmetry, i.e., $\boldsymbol{\psi}_1(r) = \boldsymbol{\psi}_2^*(-r)$.

No matter whether the $\mathcal{PT}$ symmetry is broken or not, the chiral relation between the forward- and backward-propagating modes is always broken due to the existence of $\bar{\boldsymbol{\chi}}_{r,eh}$ and $\bar{\boldsymbol{\chi}}_{r,he}$. In Figs. 3(a)–3(d), the blue square symbols representing effective mode indices given by GCMT show a large discrepancy with the gray line calculated by COMSOL. It is clear that in this case, GCMT based on chiral symmetry fails to capture the major feature of bianisotropic waveguides. The red circular symbols in the same figures calculated by our GCMF match excellently well with the results from full-wave simulations. In this extreme circumstance, where both the bianisotropy and gain/loss exist in waveguide, the traditional coupled-mode theories such as CCMT and GCMT all fail due to the broken link between forward- and backward-propagating modes.

V. CONCLUSION

In conclusion, we developed a generalized coupled-mode formulation to study the mode hybridization in reciprocal waveguides, in which the anisotropy and the bianisotropy play an essential role. In our description, the waveguide problem is reformulated as a generalized eigenvalue problem as the original system, accompanied by the its adjoint generalized eigenvalue problem as its dual partner. The two complementary systems together define the dual mode sets, which are needed in constructing the GCMF. In reciprocal waveguides, we find out that the symmetry relations between the dual mode sets are dictated by the *same-β argument* and the *pairing-β argument*, which turns out to be intimately related with the forward- and backward-propagating modes. Accordingly, GCMF that can be reduced to the existing coupled-mode schemes, is realized by treating the forward- and backward-propagating modes on the same footing in the modal expansion set. Importantly, the GCMF developed here handles the modal coupling in anisotropic and bianisotropic waveguides, where the existing coupled-mode schemes fail. We illustrate the capability of our GCMF through three examples, i.e., anisotropic waveguide, bianisotropic waveguides, and bianisotropic waveguides with balanced gains and losses. The three examples unambiguously show the feasibility and the strength of our theory in studying the mode hybridization in waveguides with the broken link between the forward- and backward-propagating modes.

ACKNOWLEDGMENTS

This work was supported in part by National Natural Science Foundation of China (Grants No. 11874026, No. 61775063, and No. 61735006), National Key Research and Development Program of China (Grant No. 2017YFA0305200), and the Fundamental Research Funds for the Central Universities, HUST: 2017KFYXJJ027.

APPENDIX A: THE PROOF OF *SAME-β* ARGUMENT

We consider the dual waveguide systems described by the two equations,

$$\bar{\boldsymbol{L}}\boldsymbol{\Phi}_1 = \beta_1\bar{\boldsymbol{B}}\boldsymbol{\Phi}_1, \tag{A1}$$

$$\bar{\boldsymbol{L}}^a\boldsymbol{\Psi}_2 = \beta_2\bar{\boldsymbol{B}}^a\boldsymbol{\Psi}_2. \tag{A2}$$

To find the relation between eigenvalue β_1 and β_2, the biorthogonal basis $[\boldsymbol{\phi}_i]$, $[\boldsymbol{\psi}_j]$ is used as a basis to represent the above differential operator. The matrix elements of the operator in the $[\boldsymbol{\phi}_i]$, $[\boldsymbol{\psi}_j]$ basis are easily obtained by applying the standard Galerkin moment method as follows:

$$\bar{\bar{\boldsymbol{L}}}_{ij} = \iint \boldsymbol{\psi}_i^T\bar{\boldsymbol{L}}\boldsymbol{\phi}_j\,dxdy, \tag{A3}$$

$$\bar{\bar{\boldsymbol{L}}}^a_{ij} = \iint \boldsymbol{\phi}_i{}^T\bar{\boldsymbol{L}}^a\boldsymbol{\psi}_j\,dxdy, \tag{A4}$$

$$\bar{\bar{\boldsymbol{B}}}_{ij} = \iint \boldsymbol{\psi}_i{}^T\bar{\boldsymbol{B}}\boldsymbol{\phi}_j\,dxdy, \tag{A5}$$

$$\bar{\bar{\boldsymbol{B}}}^a_{ij} = \iint \boldsymbol{\phi}_i{}^T\bar{\boldsymbol{B}}^a\boldsymbol{\psi}_j\,dxdy, \tag{A6}$$

where $\bar{\bar{\boldsymbol{L}}}$, $\bar{\bar{\boldsymbol{L}}}^a$, $\bar{\bar{\boldsymbol{B}}}$, $\bar{\bar{\boldsymbol{B}}}^a$ are matrix representation. Transposing adjoint relation Eq. (11), one could derive

$$\iint \boldsymbol{\phi}_i^T\bar{\boldsymbol{L}}^T\boldsymbol{\psi}_j\,dxdy = \iint \boldsymbol{\phi}_i^T\bar{\boldsymbol{L}}^a\boldsymbol{\psi}_j\,dxdy. \tag{A7}$$

Due to that $\bar{\bar{\boldsymbol{L}}}_{ij}$ is a scalar, one can transpose it without changing value,

$$\bar{\bar{\boldsymbol{L}}}_{ij} = \iint \boldsymbol{\phi}_j{}^T\bar{\boldsymbol{L}}^T\boldsymbol{\psi}_i\,dxdy, \tag{A8}$$

and subsequently we shall obtain

$$\bar{\bar{\boldsymbol{L}}}_{ji} = \iint \boldsymbol{\phi}_i{}^T\bar{\boldsymbol{L}}^T\boldsymbol{\psi}_j\,dxdy. \tag{A9}$$

Identifying the three equations, i.e., Eqs. (A9), (A2), and (A7), one obtains

$$\bar{\bar{\boldsymbol{L}}}_{ji} = \bar{\bar{\boldsymbol{L}}}^a_{ij}, \tag{A10}$$

which gives rise to the symmetric relation as

$$\bar{\bar{\boldsymbol{L}}}^a = (\bar{\bar{\boldsymbol{L}}})^T. \tag{A11}$$

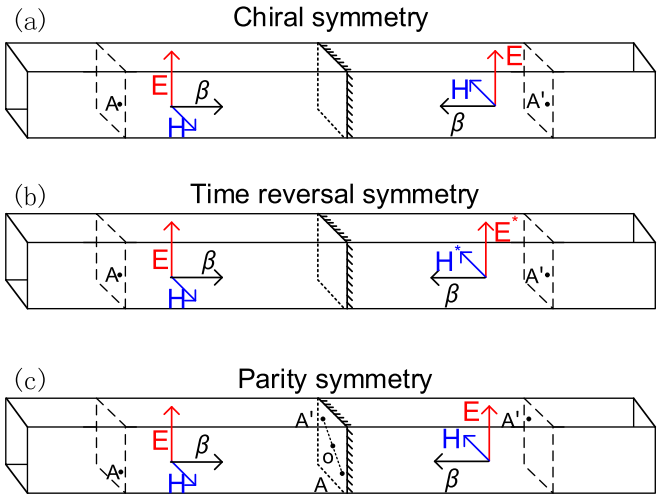

FIG. 4. The symmetry relations between the forward- and backward-propagating modes. A represents a point on the reference plane of the cross section for the forward-propagating mode, and A' represents the corresponding point on the reference plane for the backward-propagating mode. In (a) and (b), A and A' share the same coordinates in x-y plane [$\boldsymbol{r}(x,y)=\boldsymbol{r}'(x,y)$], while in (c), A and A' are symmetric about the center [$\boldsymbol{r}(x,y)=-\boldsymbol{r}'(x,y)$]. $\boldsymbol{E}$ and $\boldsymbol{H}$ stands for the transverse component of electromagnetic field, and asterisk $*$ stands for the operation of complex conjugate. The middle mirror represents the symmetry plane of the forward- and backward-propagating modes.

As for $\bar{\boldsymbol{B}}$, one easily derives

$$\bar{\bar{\boldsymbol{B}}}^a=(\bar{\bar{\boldsymbol{B}}})^T=-\bar{\bar{\boldsymbol{B}}}. \tag{A12}$$

Reformulating Eqs. (A1) and (A2) into matrix forms, one immediately obtains

$$\bar{\bar{\boldsymbol{L}}}\boldsymbol{\Phi}_1=\beta_1\bar{\bar{\boldsymbol{B}}}\boldsymbol{\Phi}_1, \tag{A13}$$

$$\bar{\bar{\boldsymbol{L}}}^a\boldsymbol{\Psi}_2=\beta_2\bar{\bar{\boldsymbol{B}}}^a\boldsymbol{\Psi}_2. \tag{A14}$$

The eigenvalue equations of Eqs. (A13) and (A14) are $|\bar{\bar{\boldsymbol{L}}}-\beta_1\bar{\bar{\boldsymbol{B}}}|=0$ and $|(\bar{\bar{\boldsymbol{L}}})^T+\beta_2\bar{\bar{\boldsymbol{B}}}|=0$, which are essentially the same via a transpose operation. Therefore, we derive the *same-β argument*, i.e., $\beta_1=\beta_2$, which states that the original and adjoint waveguide systems share the same propagation constants β.

APPENDIX B: SYMMETRY OF FORWARD AND BACKWARD PROPAGATING MODES

Time-reversal symmetry, chiral symmetry, and parity symmetry are usually used to connect the backward- and forward-propagating modes which are shown in Fig. 4. Rightward and leftward directions of vector β represent the forward- and backward-propagating modes, respectively, and their opposite directions of β indicate the *pairing-β* argument which is always satisfied in reciprocal medium. In Figs. 4(a)–4(b), the points A and A' share the same coordinates in the plane (x-y plane) perpendicular to the propagation direction, i.e., $\boldsymbol{r}_A(x,y)=\boldsymbol{r}_{A'}(x,y)$, while in Fig. 4(c) they are centrosymmetric about the central point o of cross section, i.e., $\boldsymbol{r}_A(x,y)=-\boldsymbol{r}_{A'}(x,y)$.

Chiral symmetry can be used for the cases where the material tensors of the waveguide have no off-diagonal terms, see material constraints in Table II. Figure 4(a) shows the chiral symmetry visually where the transversal electric fields are similar and the transversal magnetic fields are opposite. Time-reversal symmetry is satisfied when the material contains no loss or gain, i.e., the material tensor is a real number, and it is shown in Fig. 4(b), where the electromagnetic fields satisfy the relation $\boldsymbol{E}^+=(\boldsymbol{E}^-)^*$ and $\boldsymbol{H}^+=-(\boldsymbol{H}^-)^*$. As the distribution of refractive index of the waveguide satisfies the condition $\bar{\boldsymbol{\varepsilon}}_r(x,y,z)=\bar{\boldsymbol{\varepsilon}}_r(-x,-y,z)$, parity symmetry shown in Fig. 4(c) is valid, where the electromagnetic fields satisfy the relation $\boldsymbol{E}^+(r)=\boldsymbol{E}^-(-r)$, $\boldsymbol{H}^+(r)=-\boldsymbol{H}^-(-r)$. Detailed discussions can be found in our previous work [44]. These symmetry relations can be used in the existing coupled-mode schemes to simplify the calculation. For example, the time-reversal/chiral symmetry is an implicit assumption in CMT/GCMT for obtaining the testing modal functions.

[1] P. Paddon and J. F. Young, Phys. Rev. B **61**, 2090 (2000).
[2] S. E. Kocabas, G. Veronis, D. A. B. Miller, and S. Fan, Phys. Rev. B **79**, 035120 (2009).
[3] Y. Xu, Y. Li, R. K. Lee, and A. Yariv, Phys. Rev. E **62**, 7389 (2000).
[4] A. W. Sbyder, J. Opt. Soc. Am. **62**, 1267 (1972).
[5] A. Yariv, J. Quantum Electron. **9**, 919 (1973).
[6] A. Hardy and W. Streifer, J. Lightwave Technol. **3**, 1135 (1985).
[7] W. Huang, J. Opt. Soc. Am. A **11**, 963 (1994).
[8] P. Chak, S. Pereira, and J. E. Sipe, Phys. Rev. B **73**, 035105 (2006).
[9] P. R. Villeneuve, S. Fan, and J. D. Joannopoulos, Phys. Rev. B **54**, 7837 (1996).
[10] B. Wu, B. Wu, J. Xu, J. Xiao, and Y. Chen, Opt. Express **24**, 16566 (2016).
[11] S. Fan, P. R. Villeneuve, J. D. Joannopoulos, M. J. Khan, C. Manolatou, and H. A. Haus, Phys. Rev. B **59**, 15882 (1999).
[12] H. A. Haus, *Waves and Fields in Optoelectronics* (Prentice-Hall, Englewood Cliffs, NJ, 1984).
[13] Y. Sivan, S. Rozenberg, and A. Halstuch, Phys. Rev. B **93**, 144303 (2016).
[14] P. T. Bowen and D. R. Smith, Phys. Rev. B **90**, 195402 (2014).
[15] R. E. Hamam, A. Karalis, J. D. Joannopoulos, and M. Soljacic, Phys. Rev. A **75**, 053801 (2007).
[16] R. Buschlinger, M. Lorke, and U. Peschel, Phys. Rev. Appl. **7**, 034028 (2017).
[17] Z. Ruan and S. Fan, Phys. Rev. A **85**, 043828 (2012).
[18] B. A. Malomed, T. Mayteevarunyoo, E. A. Ostrovskaya, and Y. S. Kivshar, Phys. Rev. E **71**, 056616 (2005).
[19] C. W. Qiu, L. Gao, J. D. Joannopoulos, and M. Soljacic, Laser Photonics Rev. **4**, 268 (2009).

[20] S. G. Johnson, P. Bienstman, M. A. Skorobogatiy, M. Ibanescu, E. Lidorikis, and J. D. Joannopoulos, Phys. Rev. E **66**, 066608 (2002).

[21] M. Carnevale, B. Crosignani, and P. Di Porto, Phys. Rev. Lett. **49**, 916 (1982).

[22] G. Sun, J. B. Khurgin, and A. Bratkovsky, Phys. Rev. B **84**, 045415 (2011).

[23] T. Iizuka and C. Martijn de Sterke, Phys. Rev. E **61**, 4491 (2000).

[24] A. Yariv, Y. Xu, R. K. Lee, and A. Scherer, Opt. Lett. **24**, 711 (1999).

[25] C. Peng, Y. Liang, K. Sakai, S. Iwahashi, and S. Noda, Phys. Rev. B **86**, 035108 (2012).

[26] E. Waks and J. Vuckovic, Opt. Express **13**, 5064 (2005).

[27] P. T. Kristensen, J. R. de Lasson, M. Heuck, N. Gregersen, and J. Mork, J. Lightwave Technol. **35**, 4247 (2017).

[28] G. Lifante, *Integrated Photonics: Fundamentals*, (Wiley, Chichester, 2003), Chap. 4.

[29] H. Liu and P. Lalanne, Nature **452**, 728 (2008).

[30] R. F. Harrington, *Field Computation by Moment Methods*, (IEEE Press, New York, 1993), Chap. 1, Sec. 3.

[31] J. M. Jin, *The Finite Element Method in Electromagnetics*, 2nd ed. (Wiley, New York, 2002), Chap. 6.

[32] H. A. Haus, W. P. Huang, S. Kawakami, and N. A. Whitaker, J. Lightwave Technol. **5**, 16 (1987).

[33] R. F. Harrington, *Time-Harmonic Electromagnetic Fields*, 2nd ed. (Wiley-IEEE Press, New York, 2001).

[34] I. Stakgold, *Boundary Value Problems of Mathematical Physics*, (SIAM, New York, 1968), Vol. 2, Chap. 8.

[35] P. Pintus, Opt. Express **22**, 15737 (2014).

[36] S. R. Cvetkovic and J. B. Davies, IEEE Trans. Microwave Theory Tech. **34**, 129 (1986).

[37] Ruey-Beei Wu and Chun Chen, IEEE Trans. Antennas Propag. **34**, 640 (1986).

[38] V. H. Rumsey, Phys. Rev. **94**, 1483 (1954).

[39] W. C. Chew, IEEE Trans. Antennas Propag. **56**, 970 (2008).

[40] N. Moiseyev, *Non-Hermitian Quantum Mechanics* (Cambridge University Press, New York, 2011), Chap. 6.

[41] D. Marcuse, Bell Syst. Tech. J. **54**, 985 (1975).

[42] S. L. Chuang, J. Lightwave Technol. **5**, 5 (1987).

[43] J. Xu and Y. Chen, Opt. Express **23**, 22619 (2015).

[44] Z. F. Xiong, W. J. Chen, P. Wang, and Y. T. Chen, Opt. Express **23**, 29822 (2017).

[45] Y. Xu and R. G. Bosisio, IEEE Trans. Microwave Theory Tech. **43**, 873 (1995)

[46] Y. Xu and R. G. Bosisio, Microwave Opt. Technol. Lett. **12**, 279 (1996).

[47] Y. Xu and R. G. Bosisio, Microwave Opt. Technol. Lett. **14**, 308 (1997).

[48] J. Pitarch, J. M. Catalá-Civera, F. L. Peñaranda-Foix, and M. A. Solano, IEEE Trans. Microwave Theory Tech. **55**, 108 (2007)

[49] J. Xu, B. Wu, and Y. Chen, Opt. Express **23**, 11566 (2015).

[50] J. J. Sakurai and S. F. Tuan, *Modern Quantum Mechanics*, Rev. ed (Addison-Wesley Pub. Co, Reading, Mass, 1994).

[51] R. E. Collin, *Field Theory of Guided Waves*, (The Maple Press, New York, 1960), Chap. 6, p. 231.

[52] P. R. McIsaac, IEEE Trans. Microwave Theory Tech. **39**, 1808 (1991).

[53] A. T. Villeneuve, IEEE Trans. Microwave Theory Tech. **7**, 441 (1959).

[54] E. Silvestre *et al.*, IEEE Trans. Microwave Theory Tech. **48**, 589 (2000).

[55] A. W. Snyder and J. D. Love, *Optical Waveguide Theory* (Springer Science & Business Media, New York, 2012).

[56] Y. Zhu and A. C. Cangellaris, *Multigrid Finite Element Methods for Electromagnetic Field Modeling* (Wiley-IEEE, Hoboken, N.J., 2006), Chap. 8, Sec. 4.

[57] http://www.comsol.com

[58] K. Y. Bliokh, D. Smirnova, and F. Nori, Science **348**, 1448 (2015).

[59] H. Benisty, C. Yan, A. Degiron, and A. Lupu, J. Lightwave Technol. **30**, 2675 (2012).

[60] S. Klaiman, U. Gunther, and N. Moiseyev, Phys. Rev. Lett. **101**, 080402 (2008).

[61] P. Chen and Y. D. Chong, Phys. Rev. A **95**, 062113 (2017).